POLITECNICO DI TORINO
Repository ISTITUZIONALE

Direct Flux and Torque Control of Electrically Excited Synchronous Traction Motors

Original
Direct Flux and Torque Control of Electrically Excited Synchronous Traction Motors / Ionta, A., Rubino, S., Graffeo, F., Mandrile, F., Bojoi, R., Armando, E.. - In: IEEE TRANSACTIONS ON INDUSTRY APPLICATIONS. - ISSN 0093-9994. - (2026), pp. 1-15. [10.1109/tia.2026.3675223]

Availability:
This version is available at: 11583/3008907 since: 2026-03-19T08:49:22Z

Publisher:
IEEE

Published
DOI:10.1109/tia.2026.3675223

Terms of use:

This article is made available under terms and conditions as specified in the corresponding bibliographic description in the repository

Publisher copyright
IEEE postprint/Author's Accepted Manuscript

©2026 IEEE. Personal use of this material is permitted. Permission from IEEE must be obtained for all other uses, in any current or future media, including reprinting/republishing this material for advertising or promotional purposes, creating new collecting works, for resale or lists, or reuse of any copyrighted component of this work in other works.

(Article begins on next page)

18 November 2026

This article has been accepted for publication in IEEE Transactions on Industry Applications. This is the author's version which has not been fully edited and content may change prior to final publication. Citation information: DOI 10.1109/TIA.2026.3675223

Direct Flux and Torque Control of Electrically Excited Synchronous Traction Motors

Alessandro Ionta, *Student member, IEEE*, Sandro Rubino, *Member, IEEE*, Federica Graffeo, *Member, IEEE*, Fabio Mandrile, *Member, IEEE*, Radu Bojoi, *Fellow, IEEE* and Eric Armando, *Senior Member, IEEE*

***Abstract*—Permanent Magnet Synchronous Machines (PMSMs) utilizing rare-earth magnets are currently the most prevalent solution for electric powertrains due to their high torque density and efficiency. However, Electrically Excited Synchronous Machines (EESMs) have emerged as a viable alternative for automotive powertrains to reduce the reliance on rare-earth materials. Indeed, the EESMs offer a higher degree of freedom compared to PMSMs, as the machine flux can be regulated through the rotor field current. However, the literature provides few torque control solutions for EESM with optimal torque production, primarily based on current vector control (CVC) algorithms. Therefore, this article presents a torque controller based on the Direct Flux Vector Control (DFVC) approach for highly saturated EESMs used in traction applications. The proposed torque controller is based on a total copper loss-minimizing approach. At the same time, it fastly regulates the torque with high performance regardless of the rotor excitation dynamics. Furthermore, the proposed torque controller can deal with variable stator and rotor current limits, allowing the potential implementation of the thermal strategies reported in the literature. Experimental results obtained on a commercial 100 kW EESM employed by the Renault Zoe EV R135 are reported, validating the proposed torque controller's performance.**

***Index Terms*—direct flux vector control, electrically excited synchronous machine, electric vehicles, torque control.**

I. Introduction

PERMANENT Magnet Synchronous Machines (PMSMs) are currently the most widely used solution for electric vehicles due to their high torque density and efficiency [1], [2]. However, the dependence on rare-earth materials has driven engineers to seek alternative machines without magnets. The Electrically Excited Synchronous Machine (EESM) has recently garnered interest as an alternative technology for traction applications since it does not require permanent magnets (PMs). This type of machine, also known as wound field synchronous machine, includes a dc-supplied winding in the rotor that generates the excitation field without PMs, thereby avoiding the risks of demagnetization and uncontrolled generation [3]. Additionally, the EESM offers an extra degree of freedom, as the machine flux can be regulated through the rotor field current. This enables constant power over a wide speed range and excellent flux-weakening capability with high efficiency [4]. As a result, many carmakers consider today the EESM as a valid alternative to PMSM and start exploring its different topologies [5]. The augmented degree of freedom, introduced by the rotor current, complicates the electromagnetic design process. At each operating point within the required torque-speed range dictated by the vehicle driving cycle, both the stator current vector and the rotor current need to be calculated, thereby considerably enlarging the design parameters [6], [7].

The additional degree of freedom introduced by the manipulation of the rotor field current presents novel control challenges in the pursuit of optimizing torque production [8]. Limited solutions have been reported in the literature regarding EESM torque control, implementing mainly Current Vector Control (CVC) schemes regulating the dq- and rotor currents [8]–[13]. The mutual coupling between the stator d-axis and rotor axis complicates current regulation, posing significant challenges for effective control [14], emphasizing the need to fully leverage the capabilities of the machine.

In EESMs designed for Electric Vehicles (EVs), the exciter inductance is typically significantly larger than the stator inductances, often by several orders of magnitude. As a result, the exciter dynamics exhibit a considerably slower response compared to the stator, even when the rotor controller tries to force all the available rotor voltage. The trade-off between efficiency-optimized operating points, requiring adjustments in the exciter current, and the inherently low exciter dynamic, leads to a reduction in torque response [11]. This issue is already experienced in induction motor (IM) drives [15], which are affected by the slow dynamics of the rotor flux linkage. Like IM drives, a possible solution for EESMs considers temporarily increasing the current stator limit, allowing for a transient overload. In such cases, the torque dynamic can be enhanced by leveraging the fast response of the stator currents [12]. To obtain a solution always applicable, the magnetic coupling between stator and rotor needs to be examined [16]. A CVC scheme is discussed in [17], where the advantages of modeling the machine in a stator flux-oriented reference frame are highlighted. A deadbeat-direct torque and flux control is proposed in [18], [19], in which a field flux linkage command is derived to achieve unity power factor in the steady-state. Machine losses are not always minimized for unity power factor. Indeed, more complex algorithms to obtain a greater efficiency need to be elaborated [10]–[13], [20]–[22].

A further common challenge associated with synchronous motors' reliability is the occurrence of failures due to uncontrolled temperature increase [23]. Various methods can be utilized to conduct a detailed thermal analysis of an electric traction motor, including lumped parameter thermal network modeling and finite element analysis [24]. As highlighted in [25], the most thermally critical components are the windings, primarily due to the insulation materials used in their manufacturing. Exposure to inappropriate temperatures can reduce

Authorized licensed use limited to: Politecnico di Torino. Downloaded on March 19,2026 at 08:41:58 UTC from IEEE Xplore. Restrictions apply.
© 2026 IEEE. All rights reserved, including rights for text and data mining and training of artificial intelligence and similar technologies. Personal use is permitted, but republication/redistribution requires IEEE permission. See https://www.ieee.org/publications/rights/index.html for more information.

This article has been accepted for publication in IEEE Transactions on Industry Applications. This is the author's version which has not been fully edited and content may change prior to final publication. Citation information: DOI 10.1109/TIA.2026.3675223

the lifespan of these materials by up to 50% [26]. Therefore, effective thermal management of motor windings is crucial for EVs [26]. Employing adequate thermal strategies protects essential elements from excessive temperature increases [27]–[29]. According to the literature, these thermal strategies often consist of changing the current limits of stator- and, for EESMs, rotor windings.

According to the presented research context, this article proposes a novel torque controller for traction EESMs that overcomes the consolidated direct regulation of the stator dq-currents by implementing a Direct Flux Vector Control (DFVC) [30]–[32] scheme. The proposed torque controller brings added value to the existing literature by presenting the following features and contributions.

- The torque regulation is self-linearized over the entire torque-speed range, without requiring demanding Look-Up Tables (LUTs) as for CVC controllers.
- The torque regulation exhibits high control performance regardless of the rotor exciter dynamics, which is penalized by the large rotor inductance value.
- The steady-state torque production is characterized by high efficiency since the overall copper losses are always minimized.
- The above-mentioned features of torque regulation are also preserved for online changing of the limits for both stator and rotor currents, allowing the potential implementation of the thermal strategies reported in the literature [27]–[29].

This article builds upon the conference paper [33], where the DFVC scheme for EESM has been preliminary validated at low speed and without considering variable stator and rotor current limits. This article extends [33] by incorporating the following key aspects.

- Comprehensive details on the computation and efficient interpolation of LUTs implemented in the proposed torque controller.
- An in-depth description and analysis of the control modules implementing the variable stator and rotor current limits.
- Experimental validation of the DFVC scheme at high speed considering deep Flux-Weakening (FW) operation with Maximum Torque per Voltage (MTPV) limitation, along with an in-depth analysis of the accuracy and the achievable dynamic performance of the torque regulation.

The schematic view of the considered EESM drive topology is shown in Fig. 1. The EESM is fed on the stator by a three-phase voltage source inverter, while an exciter feeds the rotor. No assumptions are made on the rotor exciter since it can consist of a conventional dc-dc converter or any wireless typology reported in the literature [34], [35]. The torque controller generates the reference voltages v^*_{abc} for the computation of the inverter's duty-cycle commands d^*_{abc}, along with the voltage reference v^*_f for the generic exciter.

The article is organized as follows. Section II presents the machine modeling with the theoretical background, pointing out the advantages of DFVC solutions for EESMs. A detailed description of the structure of the proposed torque controller is provided in Section III, while Section IV reports the experimental validation carried out on a commercial 100 kW EESM used on the Renault Zoe EV R135. Finally, Section V concludes the article.

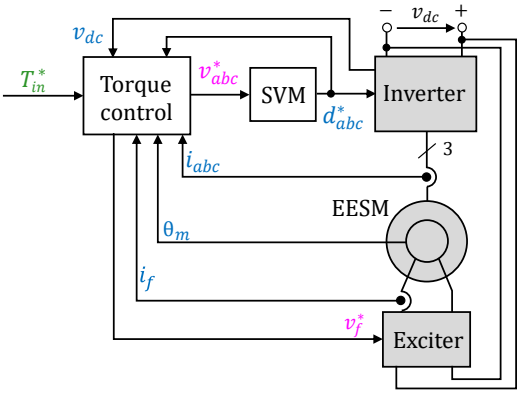


Fig. 1: Schematic view of EESM drive topology.

II. EESM MODELING

Voltage and flux linkage equations of a synchronous motor can be written in both stator (dqs) and rotor (dq) coordinates, as shown in Fig. 2. Since the DFVC scheme is implemented in rotating stator coordinates, the EESM modeling is reported in dqs reference frame [30], [33], [36].

A. Electromagnetic model in rotating coordinates

The stator voltage model (1) and torque equation (2) are common to all ac machines in the stator flux frame as:

$$\bar{v}_{dqs} = R \cdot \bar{i}_{dqs} + \frac{d}{dt} \cdot \begin{bmatrix} \lambda \\ 0 \end{bmatrix} + \lambda \cdot \begin{bmatrix} 0 \\ \omega + \frac{d\delta}{dt} \end{bmatrix} \tag{1}$$

$$T = \frac{3}{2} \cdot p \cdot \bar{\lambda} \times \bar{i} = \frac{3}{2} \cdot p \cdot \lambda \cdot i_{qs} \tag{2}$$

where the superscript " $\bar{}$ " indicates a vector, the subscripts of the stator vectors of voltage and current denote their corresponding dqs components, while λ stands for amplitude of the stator flux linkage vector, ω is the rotor synchronous speed, p is the pole pairs, and δ is the load angle, i.e., the phase angle of the stator flux with respect to the d-axis, as shown in Fig. 2.

The equation (1) indicates that the stator flux amplitude λ can be regulated through the ds-axis voltage, whereas the load angle can be controlled via the qs-axis voltage to regulate the electromagnetic torque. Nevertheless, (2) suggests that regulating the qs-axis current i_{qs} instead of the load angle δ may lead to a more straightforward and linear torque control scheme.

As previously said, EESM offers an extra degree of freedom, as the machine flux can be regulated through the rotor field current. Indeed, the rotor voltage equation is expressed as:

$$v_f = R_f \cdot i_f + \frac{d}{dt}\lambda_f \tag{3}$$

where the subscript f denotes the rotor winding variables of voltage, current, flux linkage and resistance.

Authorized licensed use limited to: Politecnico di Torino. Downloaded on March 19,2026 at 08:41:58 UTC from IEEE Xplore. Restrictions apply.
© 2026 IEEE. All rights reserved, including rights for text and data mining and training of artificial intelligence and similar technologies. Personal use is permitted, but republication/redistribution requires IEEE permission. See https://www.ieee.org/publications/rights/index.html for more information.

This article has been accepted for publication in IEEE Transactions on Industry Applications. This is the author's version which has not been fully edited and content may change prior to final publication. Citation information: DOI 10.1109/TIA.2026.3675223

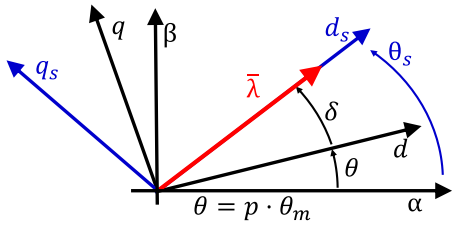


Fig. 2: Schematic view of the stationary- $\alpha\beta$, rotor- dq, and stator- dqs frames for a generic ac motor.

B. State-space model

To correlate the dqs voltages to the variables controlled by DFVC schemes (λ, i_{qs}), the corresponding state-space equations are reported in the following. The state-space equation of the flux amplitude is already computed as it corresponds to the ds-axis equation of (1), hereafter reformulated as:

$$\frac{d\lambda}{dt} = -R \cdot i_{ds} + v_{ds} \tag{4}$$

In the same way, the state-space equation of the load angle δ is straightforwardly retrieved as:

$$\lambda \cdot \frac{\delta}{dt} \simeq -R \cdot i_{qs} + v_{qs} - \omega \cdot \lambda \tag{5}$$

Equation (5) must be manipulated with a transformation of variables [36], obtaining the following state-space equation:

$$l_{qs} \cdot \frac{di_{qs}}{dt} \simeq -R \cdot i_{qs} + v_{qs} - \omega \cdot \lambda \tag{6}$$

where the qs-axis incremental inductance is computed as:

$$l_{qs} = \frac{2 \cdot l_{dd} \cdot l_{qq}}{l_{dd} + l_{qq} - (l_{qq} - l_{dd}) \cdot \cos(2 \cdot \delta)} \tag{7}$$

In (7), l_{dd} and l_{qq} are the equivalent incremental inductances along the rotor dq-axes, and whose definition corresponds to as follows [37]:

$$\begin{bmatrix} l_{dd} & l_{dq} \\ l_{qd} & l_{qq} \end{bmatrix} = \begin{bmatrix} \frac{\partial \lambda_d(i_d,i_q,i_f)}{\partial i_d} & \frac{\partial \lambda_d(i_d,i_q,i_f)}{\partial i_q} \\ \frac{\partial \lambda_q(i_d,i_q,i_f)}{\partial i_d} & \frac{\partial \lambda_q(i_d,i_q,i_f)}{\partial i_q} \end{bmatrix} \tag{8}$$

In (8), the partial derivatives are computed for a constant value of the rotor flux linkage λ_f. This hypothesis is reasonable for EESM since the time constant involving the rotor winding is typically much higher than those ruling the stator one. It is also important to note in (8) that the dq inductances depend not only on the dq currents but also on the rotor field current i_f.

Similar mathematical manipulation can be done to retrieve the rotor state-space equation to correlate the rotor voltage v_f to the controlled rotor current i_f. In this case, the equivalent rotor incremental inductance l_{ff} has to be introduced:

$$l_{ff} = \frac{\partial \lambda_f(i_d, i_q, i_f)}{\partial i_f} \tag{9}$$

By combining (3) and (9), the rotor state-space equation is straightforwardly retrieved as:

$$l_{ff} \frac{di_f}{dt} = -R_f \cdot i_f + v_f \tag{10}$$

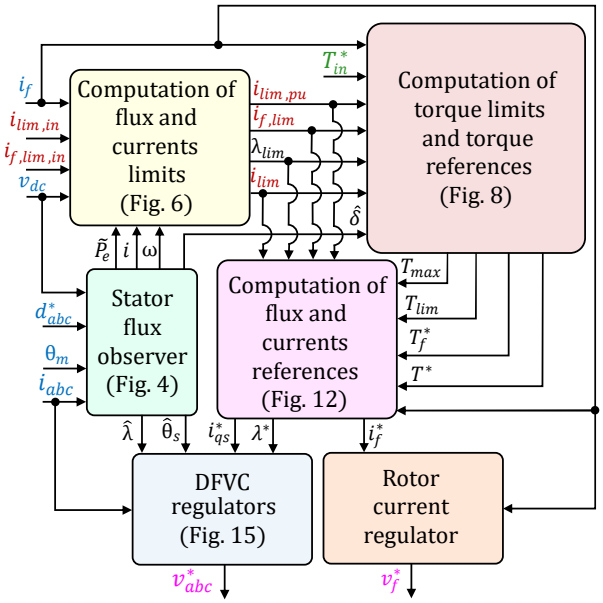


Fig. 3: Schematic view of the proposed torque controller.

C. DFVC feasibility for EESM

According to the machine model in dqs coordinates (1), (2), (3) and the corresponding state-space equations (4), (6), (10), the following advantages of DFVC schemes can be deduced.

1) Torque regulation preserves linearity across all operating conditions, including FW operation. In DFVC schemes, the qs-axis current reference is computed directly from (2) based on the flux amplitude reference, thus obviating the need of LUTs for torque linearization, which is mandatory in LUT-based CVC solutions [8]–[13].
2) Over the base speed, the FW operation is straightforward: the flux amplitude reference is limited according to the ratio between the stator voltage limit and the rotor electric speed.
3) The dynamic performance of the closed-loop control of the stator flux amplitude is invariant to the machine's operating point, evident from (4). The inner regulators for flux amplitude and qs-axis current operate with independent voltage margins; only a minimal voltage margin is required to counteract the ds-axis voltage drops attributable to stator resistance and the inverter (4). Consequently, the qs-axis regulator can exploit nearly the entire voltage range supplied by the inverter, thereby ensuring exceptionally high dynamic performance of torque regulation even under voltage constraints.
4) Avoiding the direct control of the stator d-axis current significantly mitigates the control challenges posed by the stator and rotor mutual coupling [14], thereby facilitating a more effective torque regulation.

III. DFVC-BASED TORQUE CONTROL SCHEME FOR EESM

The schematic view of the proposed torque controller is detailed in Fig. 1 and Fig. 3. According to the input torque reference T^*_{in}, the DFVC-based torque controller generates the stator reference phase voltages $v^*_{abc} = [v^*_a, v^*_b, v^*_c]$ and the

Authorized licensed use limited to: Politecnico di Torino. Downloaded on March 19,2026 at 08:41:58 UTC from IEEE Xplore. Restrictions apply.
© 2026 IEEE. All rights reserved, including rights for text and data mining and training of artificial intelligence and similar technologies. Personal use is permitted, but republication/redistribution requires IEEE permission. See https://www.ieee.org/publications/rights/index.html for more information.

This article has been accepted for publication in IEEE Transactions on Industry Applications. This is the author's version which has not been fully edited and content may change prior to final publication. Citation information: DOI 10.1109/TIA.2026.3675223

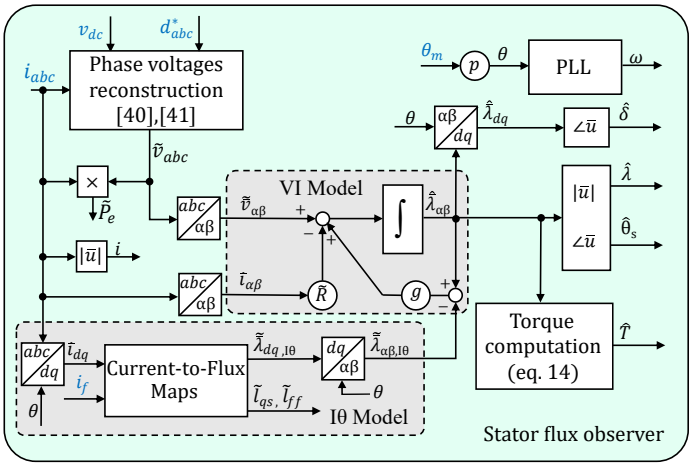


Fig. 4: Schematic view of the adopted stator flux observer.

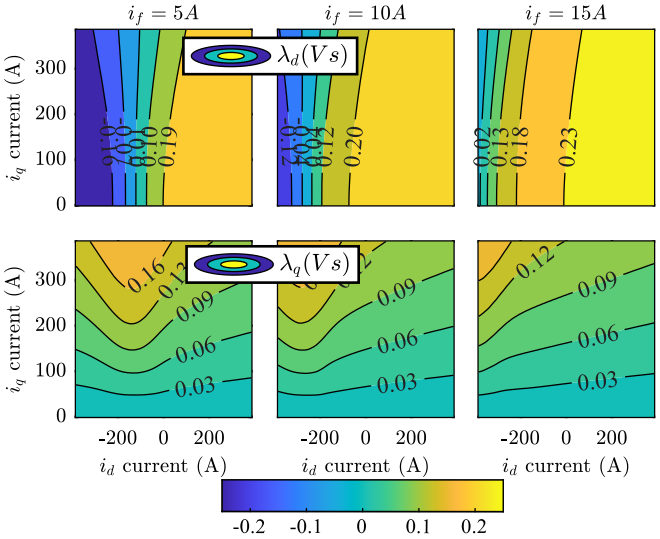


Fig. 5: Current-to-flux maps for the EESM under consideration.

rotor reference voltage v_f^* according to the following feedback quantities:

- stator phase currents $i_{abc} = [i_a, i_b, i_c]$;
- inverter's dc-link voltage v_{dc}
- rotor mechanical position θ_m
- rotor current i_f

From the reference stator phase voltages, the inverter's duty-cycles $d^*_{abc} = [d^*_a, d^*_b, d^*_c]$ are computed implementing any PWM technique [38]. This article considers carrier-based space vector modulation (SVM). As shown in Fig. 3, the developed DFVC scheme implements the following control modules:

A. Stator flux observer
B. Computation of flux and current limits
C. Computation of torque limits and torque references
D. Computation of flux and currents references
E. DFVC regulators
F. Rotor current regulator

A detailed description of the above control modules is provided in the following, along with a discussion on the implementation of LUTs necessary to deal with the strong non-linear dependence of EESM's magnetic behavior with the rotor current i_f. In the description of the control modules, the following superscripts $\tilde{}$, $\hat{}$, and * denote an estimated, observed, and reference variable/parameter, respectively. Estimated quantities arise from open-loop model propagation, while observed quantities are obtained from closed-loop observers incorporating measurement feedback.

A. Stator flux observer

The stator flux vector is estimated by implementing a consolidated flux observer structure that combines two model-based estimators [30], [39], [40], as shown in Fig. 4. The two model-based estimators are implemented in the stationary coordinates $\alpha\beta$ and designed as follows.

1) Voltage model (VI): The voltage model VI provides the flux estimate as the integral of the stator back-electromotive force voltage vector:

$$\tilde{\bar{\lambda}}_{\alpha\beta,VI} = \int (\tilde{\bar{v}}_{\alpha\beta} - \tilde{R} \cdot \bar{i}_{\alpha\beta}) dt \tag{11}$$

where $\tilde{\bar{v}}_{\alpha\beta}$ is the reconstructed voltage vector in stationary coordinates calculated from the measured inverter dc-link voltage v_{dc} and the duty-cycle commands d^*_{abc} [40], [41]. Compensation for voltage errors introduced by the inverter is suggested to improve the phase voltages reconstruction [40], [41].

2) Current model (Iθ): The current model $I\theta$ is based on the current-to-flux relationships [30], as shown in Fig. 5. According to Fig. 4, the input of this estimator are the measured stator current vector in the rotor dq coordinates and the rotor field current i_f, thus resulting immune to inverter's voltage errors, which are particularly significant in the low-speed range [39].

The final stator flux estimate is obtained as a linear combination between the voltage model VI, reliable at high speed, and the current model $I\theta$, instead reliable at low speed. The crossover frequency between the two models is equal to the observer gain g. The adopted observer structure inherently mitigates the effect of stator resistance R variation due to temperature. Indeed, the resistive voltage drops can be reasonably considered negligible at high speed, as they are much smaller than the machine's back-electromotive force. Conversely, the significant impact of resistive voltage drops at low speed is mitigated since the flux estimate of the observer coincides with that provided by the $I\theta$ estimator (immune to stator resistance variation), thanks to the observer's gain g.

With reference to Fig. 4, the flux observer outputs are the following quantities:

- Flux amplitude

$$\hat{\lambda} = \sqrt{\hat{\lambda}_\alpha^2 + \hat{\lambda}_\beta^2} \tag{12}$$

- Stator flux vector position

$$\hat{\theta}_s = \text{atan2}(\hat{\lambda}_\beta, \hat{\lambda}_\alpha) \tag{13}$$

- Load angle

$$\hat{\delta} = \text{atan2}(\hat{\lambda}_q, \hat{\lambda}_d) \tag{14}$$

Authorized licensed use limited to: Politecnico di Torino. Downloaded on March 19,2026 at 08:41:58 UTC from IEEE Xplore. Restrictions apply.
© 2026 IEEE. All rights reserved, including rights for text and data mining and training of artificial intelligence and similar technologies. Personal use is permitted, but republication/redistribution requires IEEE permission. See https://www.ieee.org/publications/rights/index.html for more information.

This article has been accepted for publication in IEEE Transactions on Industry Applications. This is the author's version which has not been fully edited and content may change prior to final publication. Citation information: DOI 10.1109/TIA.2026.3675223

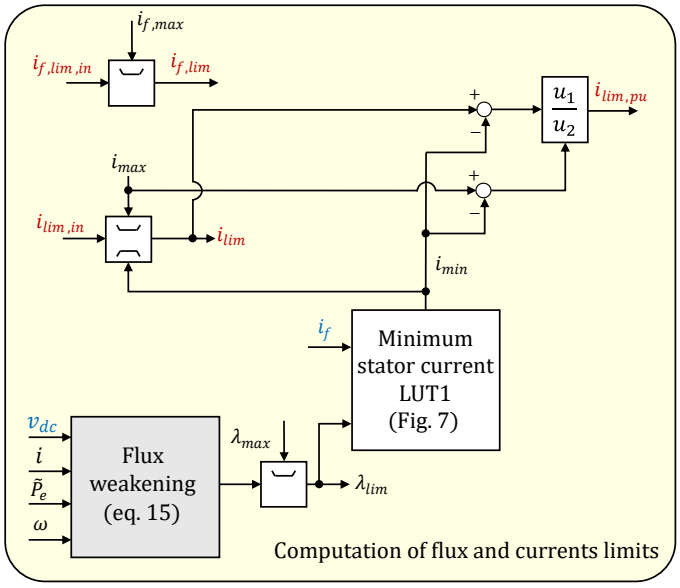


Fig. 6: Schematic view of the computation of flux and current limits.

- Observed torque

$$\hat{T} = \frac{3}{2} \cdot p \cdot (\hat{\lambda}_\alpha \cdot i_\beta - \hat{\lambda}_\beta \cdot i_\alpha) \tag{15}$$

Finally, the rotor electric speed ω is computed from the measured d-axis position using a phase-locked loop (PLL) [42].

B. Computation of flux and current limits

The torque control algorithm must comply with the constraints imposed by the considered machine and the converters (inverter and exciter) feeding it. As previously highlighted, EESMs introduce a new control variable, the rotor field current i_f. Consequently, together with the limit of stator maximum current i_{max}, the limit of maximum rotor current $i_{f,max}$ must be considered (see Fig. 6).

In the FW region, the flux amplitude λ must always be limited to prevent exceeding the voltage limit. As the speed increases, the flux limit λ_{lim} is derived according to the inverter maximum voltage employing the relationship expressed in (16), where the resistive drops are also considered.

$$\lambda_{lim} = k_{fw} \cdot \frac{\sqrt{v_{max}^2 + (\tilde{R} \cdot i)^2 - (4/3) \cdot \tilde{R} \cdot \tilde{P}_e}}{|\omega|} \tag{16}$$

In (16), $\tilde{P}_e$ represents the estimated electric power, derived from the phase currents and the reconstructed phase voltages, while i is the amplitude of the stator current vector and v_{max} is the maximum value of the phase voltages that coincide with the sinusoidal voltage limit of the inverter, i.e., $v_{dc}/\sqrt{3}$ since SVM-based PWM is adopted. The parameter k_{fw} is a scaling factor compensating for inverter voltage errors and providing an adequate voltage margin to maintain high dynamic performance of torque regulation, even under deep FW conditions. Typical values for k_{fw} lie within the range of 0.9 to 0.95.

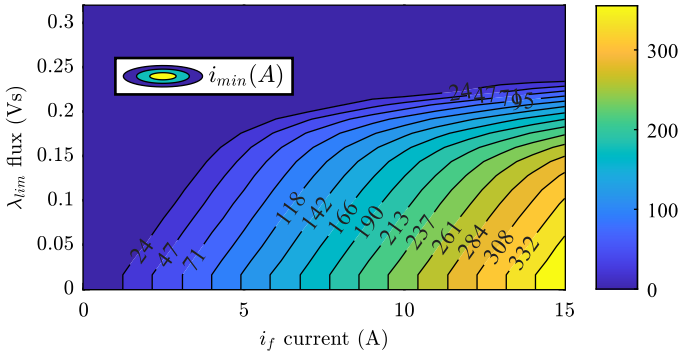


Fig. 7: Minimum stator current amplitude map (LUT1) for the EESM under consideration.

Obviously, λ_{lim} can never exceed the maximum possible flux value λ_{max} defined by the current-to-flux relationships.

Since the rotor winding typically exhibits a significant inductance, the regulation of the rotor field current i_f might not be fast enough to comply with the flux limit λ_{lim}. This is especially true if a significant rotor acceleration is requested. Therefore, in these scenarios, the flux amplitude λ has to be reduced by exploiting the faster regulation of stator quantities. Consequently, a minimum stator current amplitude i_{min} necessary to counteract the flux-producing effect of the rotor field current i_f has to be defined accordingly. In the proposed torque controller, i_{min} is provided by interpolating the 2-dimensional LUT1 (see Fig. 6), whose inputs are the measured rotor current i_f and the flux limit λ_{lim}. To facilitate the understanding, a view of LUT1 is shown in Fig. 7.

In this article, the maximum limits of stator current amplitude i_{max} and rotor current $i_{f,max}$ correspond to the most critical overload conditions of the EESM under consideration. However, these limits cannot always be considered as the effective ones during the machine's operation. Indeed, according to the literature [27], online reducing the stator and rotor current limits is mandatory to protect windings from excessive temperature levels. Therefore, an efficient derating strategy of current limits $(i_{lim}, i_{f,lim})$ is integrated into the proposed torque controller to allow the implementation of thermal strategies reported in the literature [27]–[29]. According to Fig. 6, the effective stator current amplitude limit i_{lim}, is thus obtained from the input target $i_{lim,in}$ after applying the constraints of minimum i_{min} and maximum i_{max} current amplitude. Indeed, regardless of the thermal strategy to implement, the lower limit of stator current amplitude i_{min} must be respected to guarantee the safe operability of the EESM. At the same time, the effective rotor current limit $i_{f,lim}$ is obtained from the input target $i_{f,lim,in}$ after applying the obvious constraint of maximum rotor current $i_{f,max}$. In summary, flux and currents limitations are performed with limiter blocks implementing the following constraints (see Fig. 6):

$$\begin{cases} i \le i_{lim} \quad ; \quad i_{min} \le i_{lim} \le i_{max} \\ i_f \le i_{f,lim}; \qquad i_{f,lim} \le i_{f,max} \\ \lambda \le \lambda_{lim} \end{cases} \tag{17}$$

Authorized licensed use limited to: Politecnico di Torino. Downloaded on March 19,2026 at 08:41:58 UTC from IEEE Xplore. Restrictions apply.
© 2026 IEEE. All rights reserved, including rights for text and data mining and training of artificial intelligence and similar technologies. Personal use is permitted, but republication/redistribution requires IEEE permission. See https://www.ieee.org/publications/rights/index.html for more information.

This article has been accepted for publication in IEEE Transactions on Industry Applications. This is the author's version which has not been fully edited and content may change prior to final publication. Citation information: DOI 10.1109/TIA.2026.3675223

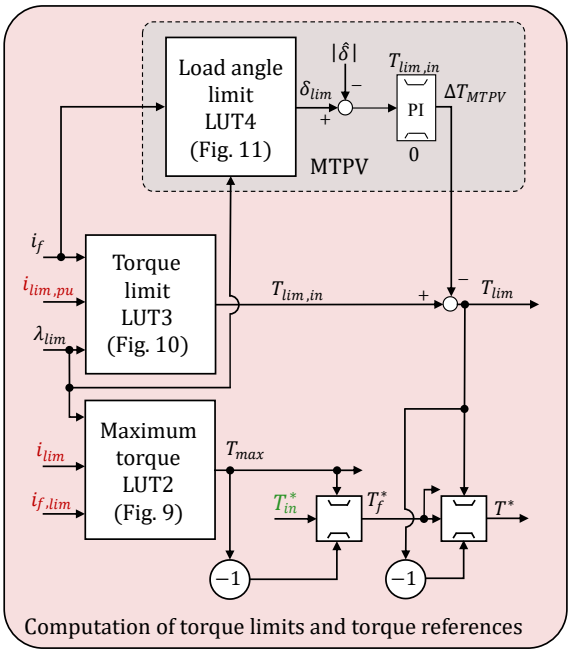


Fig. 8: Schematic view of the computation of torque limits and torque references.

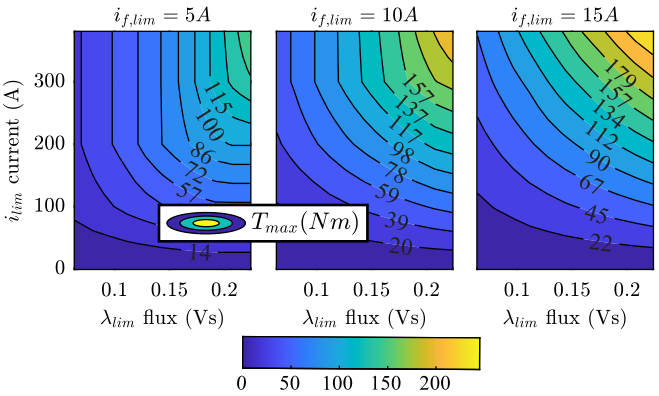


Fig. 9: Maximum torque map (LUT2) for the EESM under consideration.

C. Computation of torque limits and torque references

As previously pointed out, the primary drawback identified in the literature regarding control of traction EESMs is the exciter dynamics [11], [12], [16]. Indeed, it is well-known that the rotor current dynamics is relented by the large values of the rotor inductance. In other words, let's consider step variations of reference stator dq currents and rotor current i_f. Typically, it is reported that the rise time of the stator currents corresponding to the step excitation is considerably lower than that of the rotor current. This difference between the dynamics of stator and rotor currents hinders the dynamic performance of torque regulation. Therefore, one of this article's main contributions is the definition of a control structure that can obtain high dynamic performance of torque regulation regardless of the exciter's slow dynamic response.

For this purpose, two different torque references, one for the stator regulation T^* and one for the rotor regulation T_f^* are defined (see Fig. 8).

1) Torque reference for rotor current regulation: Starting from the generation of the torque reference for the rotor current regulation T_f^*, it is first computed the maximum torque T_{max} that the EESM under consideration can deliver according to the limits of flux amplitude λ_{lim}, rotor current $i_{f,lim}$, and stator current amplitude i_{lim}. The maximum torque T_{max} is thus obtained by interpolating the 3-dimensional LUT2, having the above limits as inputs. To facilitate the understanding, a view of LUT2 for different values of rotor current limit $i_{f,lim}$ is shown in Fig. 9. Therefore, the reference torque for the rotor current regulation T_f^* is obtained by limiting the input target torque T_{in}^* to T_{max}. It is noted that this torque limitation considers only the dynamic of the stator flux limit λ_{lim}, without considering the dynamic of the rotor current i_f.

2) Torque reference for stator quantities regulation: The generation of the torque reference for the stator quantities regulation T^* considers the limitations introduced by the measured value of the rotor current i_f and the MTPV limit, i.e., the load angle limitation δ_{lim} to avoid the EESM pull-out.

a) Torque limitation due to rotor current measurement: According to Fig. 8, the maximum achievable torque $T_{lim,in}$ is first computed based on the stator current and flux amplitude limits (i_{lim}, λ_{lim}) together with the measurement of the rotor current i_f. This torque limit is obtained by interpolating the 3-dimensional LUT3 having the aforementioned variables as inputs. However, the stator current limit i_{lim} is correlated with the values of the measured rotor current i_f and flux amplitude limit λ_{lim}, according to the minimum stator current i_{min}, as already discussed and shown in Fig. 6. This mutual correlation between the input variables of LUT3 results in a highly irregular map domain, which poses challenges for the implementation and interpolation of this LUT on digital controllers.

To address this issue, the procedure proposed in [36] is applied. A brief description of such technique is provided in the following. The directions of the map interdependent with the other ones (in this case i_{lim}), are normalized in per-unit (pu) form between 0 and 1. Here, 0 represents the minimum possible value for the considered direction given all the other ones, while 1 corresponds to its maximum. Therefore, for the implementation of LUT3, i_{lim} is normalized coherently with the value of i_{max} and $i_{min}(i_f, \lambda_{lim})$ as (see Fig. 6):

$$i_{lim,pu} = \frac{i_{lim} - i_{min}}{i_{max} - i_{min}} \tag{18}$$

This normalization enables linear multi-dimensional interpolation methods, facilitating efficient implementation on digital controllers. The graphical representation of the map's regularization process is shown in Fig. 10.

Implementing LUT3 allows for obtaining a torque limit $T_{lim,in}$ that can always be satisfied by the torque controller. Besides, this torque limit accounts for the possibility of temporarily overloading the stator windings up to i_{lim} while waiting for the rotor current to achieve its reference. This way, significant variations of the torque request can be quickly

Authorized licensed use limited to: Politecnico di Torino. Downloaded on March 19,2026 at 08:41:58 UTC from IEEE Xplore. Restrictions apply.
© 2026 IEEE. All rights reserved, including rights for text and data mining and training of artificial intelligence and similar technologies. Personal use is permitted, but republication/redistribution requires IEEE permission. See https://www.ieee.org/publications/rights/index.html for more information.

This article has been accepted for publication in IEEE Transactions on Industry Applications. This is the author's version which has not been fully edited and content may change prior to final publication. Citation information: DOI 10.1109/TIA.2026.3675223

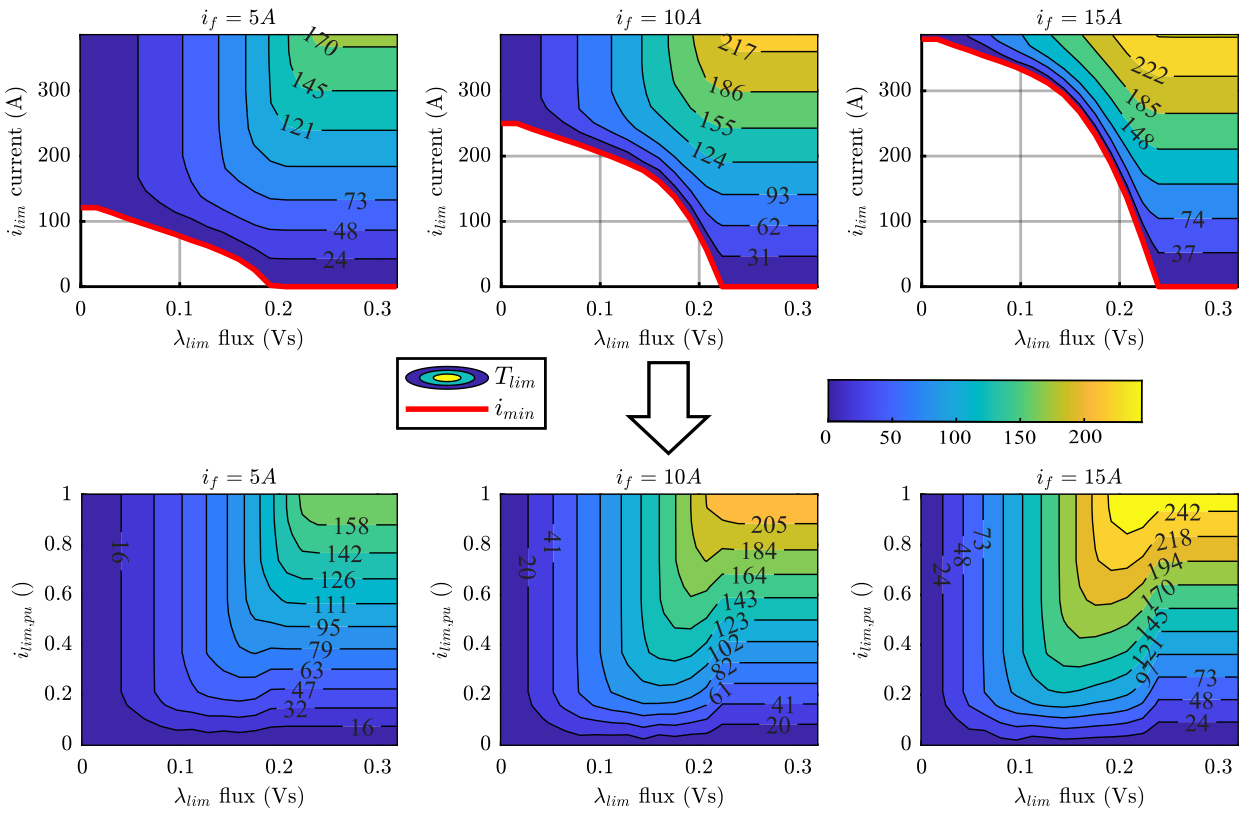


Fig. 10: Graphical view of the torque limit map (LUT3) transformation process for the EESM under consideration.

satisfied regardless of the potential slow dynamic of the rotor current.

b) Torque limitation due to MTPV: The MTPV operation occurs in deep flux-weakening operation if the stator current amplitude limit i_{lim} overcomes the EESM's characteristic current. Using a DFVC scheme, applying the MTPV limitation corresponds to appropriately limiting the machine's load angle δ [30]. Besides, this limitation is pivotal in DFVC schemes since overcoming it may lead to instability of torque regulation due to the machine's pull-out. Although the previously computed torque limit $T_{lim,in}$ automatically accounts for the MTPV operation, the DFVC scheme needs an active limitation of the machine's load angle by using an outer regulator that properly limits the torque reference [30], justifying what is shown in Fig. 8.

It is noted that an outer Proportional-Integral (PI) regulator is implemented to ensure that the estimated load angle $\hat{\delta}$ follows its limit value δ_{lim} when torque regulation would otherwise result in $\hat{\delta} > \delta_{lim}$, leading to instability. Both the limit δ_{lim} and the estimated $\hat{\delta}$ load angles must be assumed as absolute values to manage negative torque operations straightforwardly. The calibration of this PI controller is usually implemented by adopting heuristic procedures based on mathematical approximations [30]. However, regardless of the adopted calibration method, the output of this regulator, ΔT_{MTPV}, cannot overcome the torque limit due to the rotor current $T_{lim,in}$ previously computed. Indeed, by summing $T_{lim,in}$ and ΔT_{MTPV}, the absolute torque limit T_{lim} is computed. This way, the torque reference T^* for regulating the stator quantities is obtained, as shown in Fig. 6.

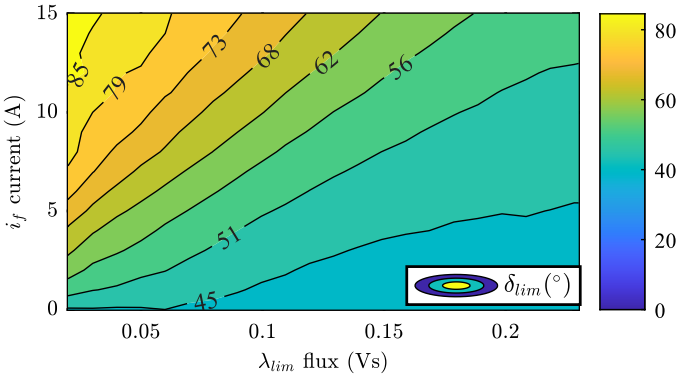


Fig. 11: Load angle limit map (LUT4) for the EESM under consideration.

Finally, in the proposed DFVC scheme, the load angle limit δ_{lim} is obtained by interpolating the 2-dimensional LUT4, whose inputs are the flux amplitude limit λ_{lim} and the measured rotor current i_f. A view of the load angle limit map is shown in Fig. 11.

D. Computation of flux and currents references

Starting from the torque reference for the stator quantities T^*, the DFVC references (λ^*, i_{qs}^*) can be retrieved. At the same time, the rotor current reference i_f^* is computed from T_f^*. According to the literature [10]–[13], [20]–[22], multiple combinations of (λ^*, i_f^*) can satisfy the torque references (T^*, T_f^*)

Authorized licensed use limited to: Politecnico di Torino. Downloaded on March 19,2026 at 08:41:58 UTC from IEEE Xplore. Restrictions apply.
© 2026 IEEE. All rights reserved, including rights for text and data mining and training of artificial intelligence and similar technologies. Personal use is permitted, but republication/redistribution requires IEEE permission. See https://www.ieee.org/publications/rights/index.html for more information.

This article has been accepted for publication in IEEE Transactions on Industry Applications. This is the author's version which has not been fully edited and content may change prior to final publication. Citation information: DOI 10.1109/TIA.2026.3675223

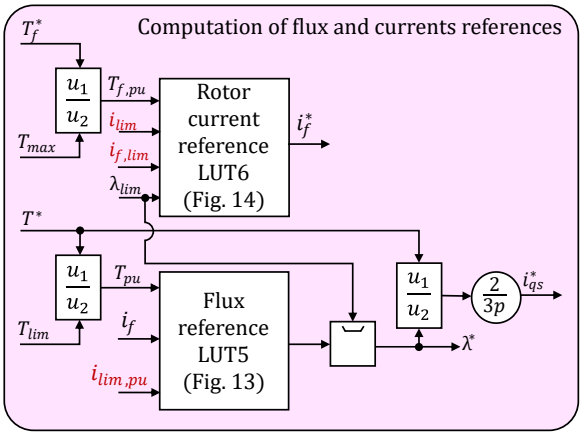


Fig. 12: Schematic view of the computation of flux and currents references.

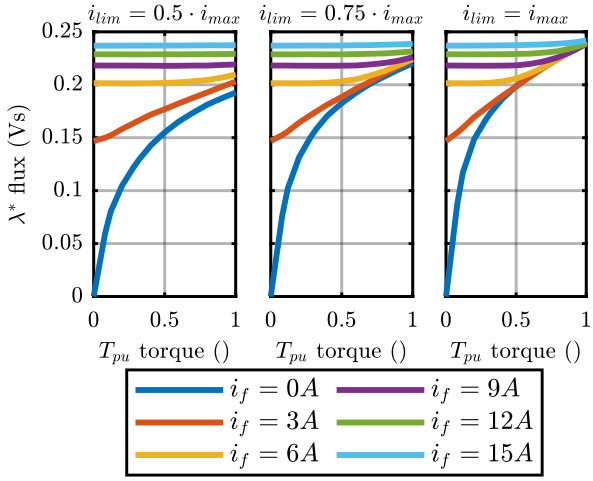


Fig. 13: Flux amplitude reference λ^* (LUT5) for different stator current limits and rotor current for the EESM under consideration.

for a specific operating speed. Common strategies like those based on Maximum Torque per Ampere (MTPA) minimize stator copper losses but neglect rotor ones. The efficiency strategy applied in the proposed torque controller considers the minimization of the total copper losses [20] comprising stator and rotor contributions. Therefore, the references (λ^*, i_f^*) are found solving the total copper losses minimization problem under the above-mentioned constraints (17) as:

$$\min_{\lambda, i_f} \left\{ \frac{3}{2} \cdot R \cdot i^2 + R_f \cdot i_f^2 \right\} \tag{19}$$

The foregoing minimization (19) is challenging since the magnetic behavior of EESMs is strongly dependent on i_f. Consequently, the minimization problem (19) is solved offline by exploiting the EESM's current-to-flux relationships, leading to the computation of LUT5 and LUT6 that provide the optimal flux amplitude reference λ^* and rotor current reference i_f^*, respectively. According to Fig. 12, torque T^* and flux amplitude λ^* references allow computing the torque-producing current reference i_{qs}^* by implementing (2). It is noted that the DFVC scheme implements a self-linearized torque regulation since the torque-producing current reference i_{qs}^* is obtained using a simple algebraic equation without using any LUT.

Following the same considerations made for the interpolation of LUT3 (Fig. 10), the linear interpolation of LUT5 and LUT6 requires the pu normalization of their respective torque references according to the corresponding maximum limits as (see Fig. 12):

$$T_{pu} = \frac{T^*}{T_{lim}}; \quad T_{f,pu} = \frac{T_f^*}{T_{max}} \tag{20}$$

A view of the flux amplitude reference map (LUT5) is shown in Fig. 13 for different values of the measured rotor current i_f and stator current amplitude limit i_{lim}. A view of the rotor current reference map (LUT6) is instead shown in Fig. 14 for different values of the measured rotor current limit $i_{f,lim}$ and stator current amplitude limit i_{lim}.

Finally, it is highlighted that this article proposes to solve the minimization problem (19) by considering the rated value of stator and rotor resistances for simplicity. However, variable

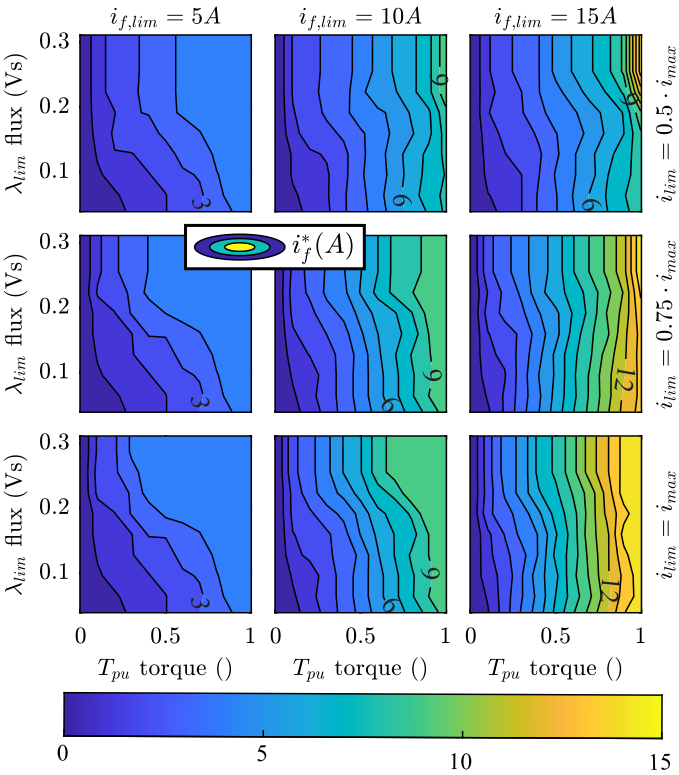


Fig. 14: Rotor current reference i_f^* maps (LUT6) for different stator and rotor current limits for the EESM under consideration.

values of stator and rotor winding temperatures can be considered by adding these as further interpolation inputs of LUT5 and LUT6. Also, it is understood that LUT5 and LUT6 can be modified to implement alternative optimization problems (e.g., minimization of copper plus iron losses) without changing the proposed control structure (Fig. 3).

Authorized licensed use limited to: Politecnico di Torino. Downloaded on March 19,2026 at 08:41:58 UTC from IEEE Xplore. Restrictions apply.
© 2026 IEEE. All rights reserved, including rights for text and data mining and training of artificial intelligence and similar technologies. Personal use is permitted, but republication/redistribution requires IEEE permission. See https://www.ieee.org/publications/rights/index.html for more information.

This article has been accepted for publication in IEEE Transactions on Industry Applications. This is the author's version which has not been fully edited and content may change prior to final publication. Citation information: DOI 10.1109/TIA.2026.3675223

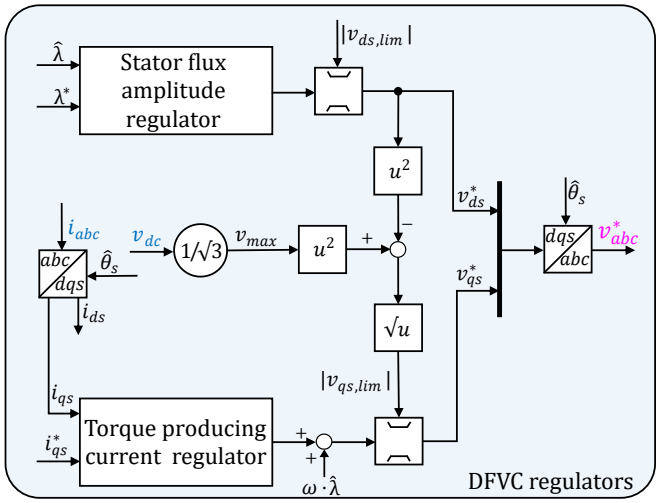


Fig. 15: Schematic view of the DFVC: closed-loop control of the stator flux amplitude and torque-producing current.

E. Direct flux vector control

The closed-loop control of stator flux amplitude λ and torque-producing current i_{qs} is performed using two regulators implemented in the stator dqs frame, as shown in the schematic view of Fig. 15.

The reference voltages in phase coordinates v^*_{abc} are then computed from those in dqs frame (v^*_{ds}, v^*_{qs}) using the Park transformation by assuming the stator flux vector position $\hat{\theta}_s$ as the rotation angle.

As highlighted in Section II-C, only a negligible voltage is required by ds-axis regulator to counteract the voltage drops related to the stator resistance and the inverter voltage errors. Hence, the voltage margin for the flux amplitude regulation $v_{ds,lim}$ can be set by following the rule of thumb law suggested in [36] as:

$$2 \cdot R \cdot i_{max} \leq v_{ds,lim} \leq 5 \cdot R \cdot i_{max} \tag{21}$$

This way, the torque-producing current regulator can dispose nearly the full voltage range provided by the inverter, thereby enabling exceptionally high dynamic performance of torque regulation even in deep FW operation. To further improve the dynamic performance of torque regulation, the compensation of the machine's back-electromotive force $(\omega \cdot \hat{\lambda})$ is suggested (see Fig. 15).

Recalling (4), it is evident that the flux amplitude controller is independent of the machine's working point. Thus, if a PI flux regulator is applied, it does not need any tuning, and its design can be performed as in [36]. Conversely, the performance of i_{qs} control loop depends on the saturation of the incremental inductance l_{qs} according to (6). Therefore, the parameters of the torque-producing current regulator should be adapted to the machine's operating point, avoiding underdamped or instability phenomena. Hence, an estimation of the incremental inductance $\tilde{l}_{qs}$ is retrieved from the current-to-flux relationships in the flux observer (see Fig. 4) to dynamically tune the parameters of the qs-axis regulator, as is shown in Fig. 16.

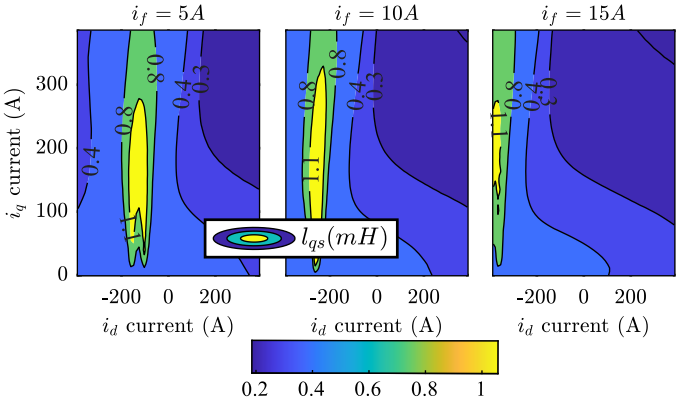


Fig. 16: Current-to-inductance l_{qs} map for the EESM under consideration.

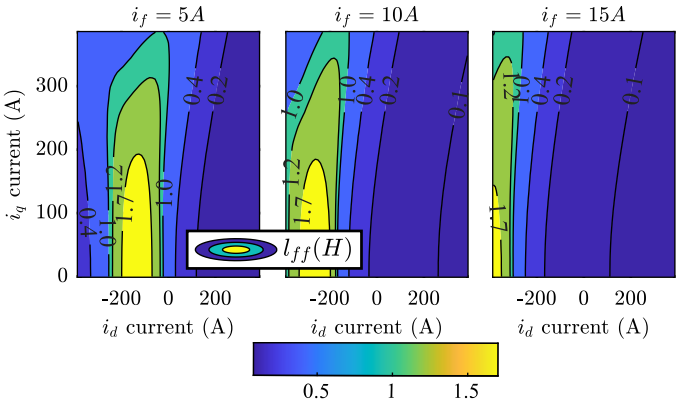


Fig. 17: Current-to-inductance l_{ff} map for the EESM under consideration.

F. Rotor current regulator

Recalling (10), it can be noted that, the performance of the rotor current i_f control loop depends on the saturation of the incremental inductance l_{ff}. Therefore, like the qs-axis regulator, the estimation of the incremental inductance $\tilde{l}_{ff}$ is retrieved in the flux observer (see Fig. 4) to tune the corresponding rotor current regulator, as shown in Fig. 17.

IV. Experimental Validation

The experimental validation of the proposed DFVC has been performed using a commercial sample of the EESM employed on the Renault Zoe EV R135 as Machine Under Test (MUT), whose primary data are listed in TABLE I.

A. Test rig

The MUT was tested in torque control mode with its shaft connected to a Driving Machine (DM) acting as a prime mover, as shown in Fig. 18. To validate the torque control algorithm, the torque sensor T12HP from HBK has been placed between the MUT and DM. The MUT was powered by an Insulated Gate Bipolar Transistor (IGBT) inverter (750V, 800A), supplied at 350 V by a bidirectional dc source. The switching frequency of the inverter has been set to 10 kHz, with a dead time of 1 μs. The rotor winding of the MUT is

Authorized licensed use limited to: Politecnico di Torino. Downloaded on March 19,2026 at 08:41:58 UTC from IEEE Xplore. Restrictions apply.
© 2026 IEEE. All rights reserved, including rights for text and data mining and training of artificial intelligence and similar technologies. Personal use is permitted, but republication/redistribution requires IEEE permission. See https://www.ieee.org/publications/rights/index.html for more information.

This article has been accepted for publication in IEEE Transactions on Industry Applications. This is the author's version which has not been fully edited and content may change prior to final publication. Citation information: DOI 10.1109/TIA.2026.3675223

TABLE I: Primary data of the EESM under test

Pole number	4
Peak power	100 kW
Peak torque	245 Nm
Rated power	51 kW
Maximum speed	11000 r/min
Rated dc-link voltage	350 V
Maximum flux (λ_{max})	0.24 Vs
Peak stator current (i_{max})	385 A
Peak rotor current ($i_{f,max}$)	15 A

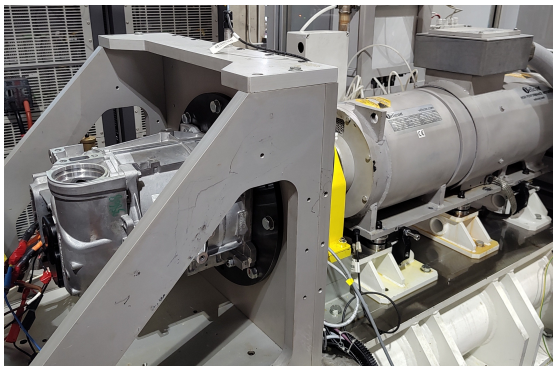


Fig. 18: View of the test rig: EESM under test (left), driving machine (right).

fed through a conventional wired system based on slip rings and brushes. The rotor exciter consisted of a SiC-based power module configured as an H-bridge [35] operating at 350 V from the same dc source used for the stator inverter. The switching frequency of the exciter has been set to 20 kHz.

The digital controller consisted of a dSPACE MicroLabBox unit for the stator inverter, while the exciter has a dedicated control board mounted on the top of the power board, housing a STM32G4 MCU that implements the measurements, generates the PWM signals to operate the switches and receives the reference rotor current i_f^* via CAN communication with the dSPACE unit. The control algorithm has been developed in MATLAB/Simulink, with automatic C-code generation performed by the dSPACE controller, and whose sampling frequency has been set to 10 kHz.

Due to the mechanical limits of the test rig, the maximum torque and speed of the MUT have been limited at 150 Nm and 10000 r/min, respectively. However, these limitations allowed to test the peak power region of the MUT, i.e., 100 kW from the base speed.

B. Experimental results

The proposed torque controller has been experimentally validated by executing several tests to verify the following requirements.

- Capability of the torque controller to manage the high torque/power operating regions of the MUT, including deep FW operation with MTPV limitation.
- Verification of the high-performance of torque regulation in the full speed range.
- Verification of the torque regulation linearity, i.e., proper limitation of the torque reference according to voltage and currents constraints and steady-state torque accuracy.
- Capability of the torque controller to deal with variable limits of rotor and stator currents by keeping high-performance of torque regulation.

According to the above requirements, the following tests have been performed.

1) *Maximum torque per speed (MTPS) profile*
2) *Fast torque reversals*
3) *Steady-state torque accuracy*
4) *Variable current limits*
5) *MTPV limitation*

Each of the above tests has been performed by setting the theoretical small-signal bandwidth of the stator control loops equal to 200 Hz, and for the rotor control loop equal to 400 Hz (PI regulators have been implemented). The observer gain g has been set to 20 Hz while the voltage margin factor for the FW operation has been set to $k_{fw} = 0.9$. The LUTs employed in the DFVC scheme were computed from the experimentally derived current-to-flux maps of the EESM under test [43], [44]. The input variables were discretized as follows: rotor current i_f from 0 to 15 A ($i_{f,max}$) with 1 A step, 16 points (pt); flux limit λ_{lim} from 0 to 0.24 Vs (λ_{max}) with 0.01 Vs step, 25 pt; stator current limit i_{lim} from 0 to 385 A (i_{max}) with 11 A step, 36 pt; rotor current limit $i_{f,lim}$ from 0 to 15 A ($i_{f,max}$) with 1 A step, 16 pt; finally all the pu quantities ($i_{lim,pu}, T_{pu}, T_{f,pu}$) from 0 to 1 with a 0.1 step, 11 pt. Therefore, the dimensions of the LUTs were: LUT1 16×25, LUT2 25×36×16, LUT3 25×11×16, LUT4 25×16, LUT5 11×11×16, LUT6 11×25×36×16. The total memory required for the LUTs is approximately 1 MB. The control algorithm achieved an execution time of 35 μs on the dSPACE platform, without applying any computational effort optimizations to the generated C code. Consequently, the implementation of this DFVC scheme is also feasible on automotive-grade MCUs. Moreover, it is highlighted that the LUTs' resolution affects the torque controller's performance only slightly when computing optimal references for the stator flux amplitude λ^* and the rotor current i_f^*, due to unavoidable approximations introduced by LUTs interpolation. However, torque regulation accuracy is preserved, with only a slight impact on the machine's efficiency. Indeed, the added value of the proposed torque controller in computing the reference of torque-producing current i_{qs}^* according to that of stator flux amplitude λ^* (see Fig. 12) automatically ensures immunity of torque regulation accuracy from LUTs' resolution.

1) MTPS profile: Starting from standstill, the speed has been changed from zero to the test rig speed limit (10000 r/min) using the DM, with an imposed acceleration of about 230 r/min/s chosen to obtain a quasi-steady-state MTPS profile. In parallel, the input reference torque T_{in}^* for the MUT controller has been set to the maximum limit (150 Nm). The current limits ($i_{lim}, i_{f,lim}$) have been imposed equal to the peak values reported in TABLE I. The MTPS profile has been tested in both motoring and braking operations. The results of the MTPS profiles are shown in Fig. 19 and Fig. 20, where P_m

Authorized licensed use limited to: Politecnico di Torino. Downloaded on March 19,2026 at 08:41:58 UTC from IEEE Xplore. Restrictions apply.
© 2026 IEEE. All rights reserved, including rights for text and data mining and training of artificial intelligence and similar technologies. Personal use is permitted, but republication/redistribution requires IEEE permission. See https://www.ieee.org/publications/rights/index.html for more information.

This article has been accepted for publication in IEEE Transactions on Industry Applications. This is the author's version which has not been fully edited and content may change prior to final publication. Citation information: DOI 10.1109/TIA.2026.3675223

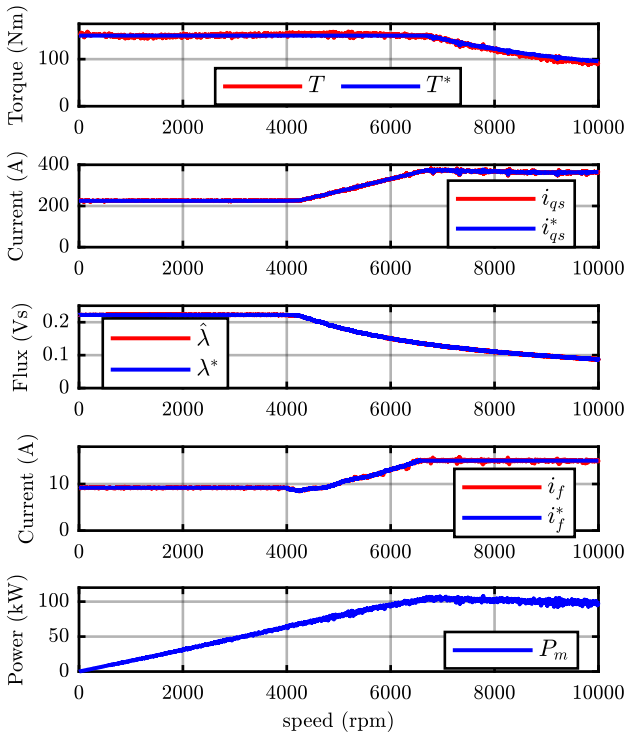


Fig. 19: MTPS profile at motoring: experimental results.

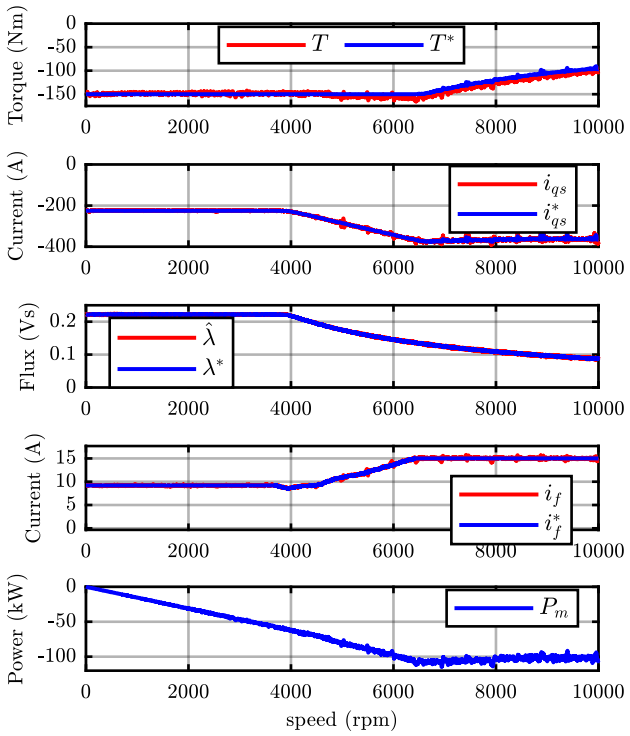


Fig. 20: MTPS profile at braking: experimental results.

is the mechanical power retrieved from the torque and speed measured by the torque sensor.

It is noted that regardless of the MTPS profile in motoring or braking operation, the proposed torque controller can fully exploit the MUT's maximum power capability in the full speed range. It is noted that all the DFVC and rotor quantities ($\hat{\lambda}, i_{qs}, i_f$) are efficiently regulated according to the total copper losses minimization strategy. According to this strategy, Fig. 19 and Fig. 20 show that FW operation is not performed by reducing the rotor current since this must be even increased to guarantee the maximum torque production. Therefore, like PMSMs, the FW operation with maximum torque of traction EESMs is still convenient to be performed by injecting negative d-axis stator current rather than reducing the rotor current. Indeed, reducing the rotor current to perform FW operation would significantly derate the maximum torque capability of the machine [45]. According to Fig. 20, it is reported that the maximum absolute torque in braking is slightly higher than that in motoring in FW operation. This difference is due to iron losses and resistive voltage drops, which lead to a higher electric power P_e that, in turn, allows getting a higher flux limit λ_{lim} according to (16) [30].

Finally, testing the MTPS profile assuming the EESM's current limits reported in TABLE I does not allow testing the MTPV limitation. This is confirmed by the firm constant power speed profiles shown in Fig. 19 and Fig. 20. The EESM under consideration most likely has been designed to get this feature.

2) Fast torque reversal: Fast torque reversals following the MTPS profile have been conducted to validate the dynamic performance of torque regulation. Utilizing the DM, the MUT was accelerated from standstill to the maximum rotational speed with an imposed acceleration of approximately 230 r/min/s, simultaneously requesting the maximum torque (150 Nm) as before. However, in contrast to the previous test, the input reference T_{in}^* torque was periodically reversed. The frequency of these torque reversals and the corresponding slew rate were selected in accordance with the mechanical seal constraints of the test rig, specifically 0.5 Hz and 150 Nm/s, respectively. This stress test simultaneously evaluates the MUT's motoring and braking performance along the MTPS profile. Furthermore, it validates the proposed DFVC scheme's capability to achieve rapid transitions between these two opposing operating modes across the entire speed range. It is evident that the stator flux amplitude $\hat{\lambda}$, torque-producing current i_{qs} and rotor field current i_f are effectively regulated under all operating conditions (see Fig. 21). This is still true even when executing rapid torque reversals in deep FW. Moreover, no instability issues or overcurrents are reported. Therefore, through this test, the high dynamic performance of torque regulation obtained by the proposed DFVC-based torque controller has been demonstrated.

3) Steady-state torque accuracy: The proposed torque controller's steady-state accuracy of torque regulation has been thoroughly verified. Specifically, multiple mechanical speed levels, uniformly distributed along the entire speed range with steps of 500 r/min, were tested using the DM. At each speed level, ten equally spaced torque levels were applied, ranging from zero to the maximum limit in motoring operation. The experimental results, presented in Fig. 22, confirm that the proposed torque controller ensures torque regulation linearity. Indeed, the torque error ΔT (both in absolute terms and as a percentage of T_{lim}) between the reference torque T^* and the measured value T is always not significant, also considering that the iron and mechanical losses have not been compensated

Authorized licensed use limited to: Politecnico di Torino. Downloaded on March 19,2026 at 08:41:58 UTC from IEEE Xplore. Restrictions apply.
© 2026 IEEE. All rights reserved, including rights for text and data mining and training of artificial intelligence and similar technologies. Personal use is permitted, but republication/redistribution requires IEEE permission. See https://www.ieee.org/publications/rights/index.html for more information.

This article has been accepted for publication in IEEE Transactions on Industry Applications. This is the author's version which has not been fully edited and content may change prior to final publication. Citation information: DOI 10.1109/TIA.2026.3675223

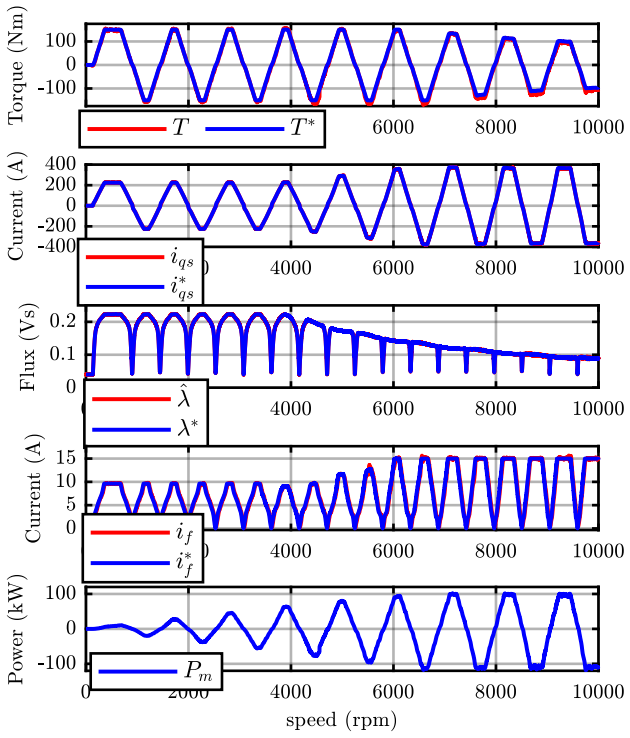


Fig. 21: Fast torque reversals along the MTPS profile: experimental results.

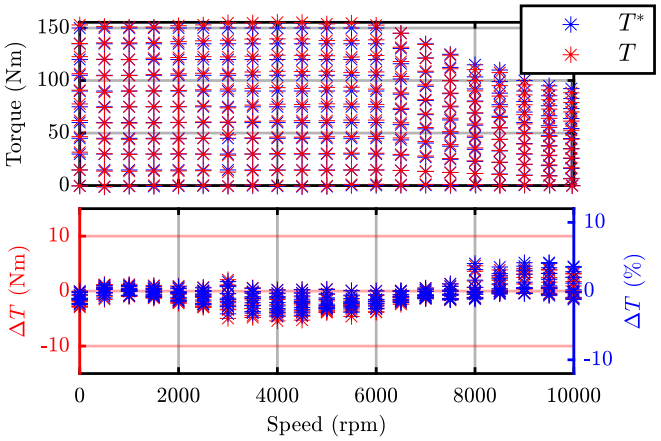


Fig. 22: Steady-state torque accuracy: experimental results.

in the computation of flux amplitude λ^* and rotor current i_f^* references.

4) Variable current limits: One of the added values of the proposed torque controller is the possibility to implement thermal strategies reported in the literature by online changing the stator i_{lim} and rotor $i_{f,lim}$ current limits. To verify this feature of the proposed torque controller, the following test has been performed. The MUT speed has been imposed to 500 r/min using the DM, while the MUT reference torque T_{in}^* has been imposed to the maximum feasible torque of 150 Nm. Initially, stator and rotor current limits have been imposed equal to the peak values reported in TABLE I ($i_{lim} = i_{max}, i_{f,lim} = i_{f,max}$). After 7.5 s from the steady-state conditions, the rotor current limit $i_{f,lim}$ has been reduced

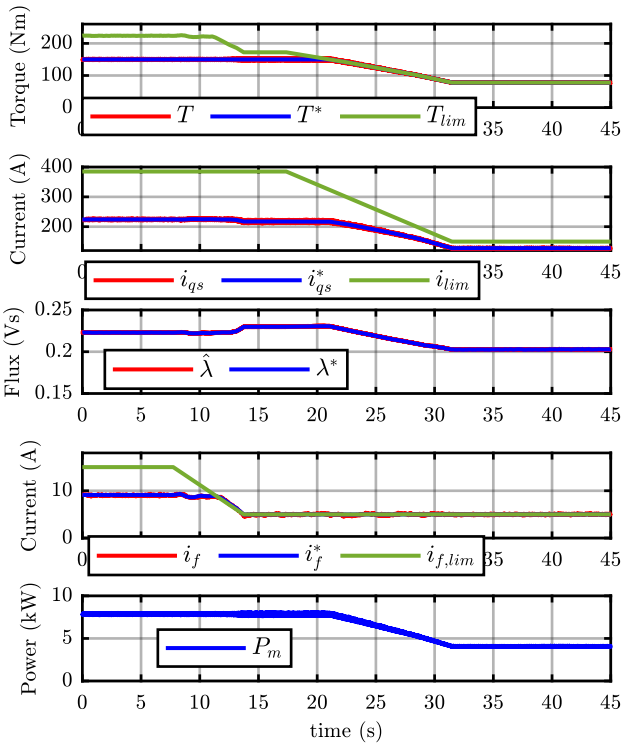


Fig. 23: Online variation of the current limits: experimental results.

from its maximum value $i_{f,max}$ =15 A to 5 A with a rate of 2 A/s. As can be noted from Fig. 23, the torque has been kept constant by the torque controller since the flux amplitude reference λ^* has been appropriately increased. Consequently, the torque-producing current reference i_{qs}^* has been online adapted according to (2). Also, it is noted that the online torque limit T_{lim} has been reduced following the reduction of the rotor current i_f. However, this torque limit reduction allowed to still imposing the input reference torque T_{in}^*. Subsequently, after 17.5 s from the test's start, also the stator current limit i_{lim} has been reduced from its maximum value i_{max} =385 A to 150 A, with a rate of 15 A/s. Compared to the previous case, the reference torque T^* is limited by the T_{lim} accordingly with the reductions of $i_{f,lim}$ and i_{lim}. However, the torque controller is still able to efficiently exploit the MUT maximum torque obtainable with the new limits, pursuing the minimization of the total copper losses.

In summary, this meaningful test has demonstrated how the proposed torque controller can straightforwardly integrate the thermal strategies for EESMs based on the online variation of stator and rotor current limits.

5) MTPV limitation: In order to test the MTPV limitation, the rotor current limit $i_{f,lim}$ has been drastically reduced to 2.5 A. This way, the maximum characteristic current of the motor has been reduced to 200 A, thus much lower than the stator current limit that has been kept at the peak value of $i_{lim} = i_{max}$ =385 A. Using these control settings, an MTPS profile in motoring has been tested. According to the rotor current limit reduction, the input torque reference has been set at 100 Nm. In parallel, using the DM, the speed has been

Authorized licensed use limited to: Politecnico di Torino. Downloaded on March 19,2026 at 08:41:58 UTC from IEEE Xplore. Restrictions apply.
© 2026 IEEE. All rights reserved, including rights for text and data mining and training of artificial intelligence and similar technologies. Personal use is permitted, but republication/redistribution requires IEEE permission. See https://www.ieee.org/publications/rights/index.html for more information.

This article has been accepted for publication in IEEE Transactions on Industry Applications. This is the author's version which has not been fully edited and content may change prior to final publication. Citation information: DOI 10.1109/TIA.2026.3675223

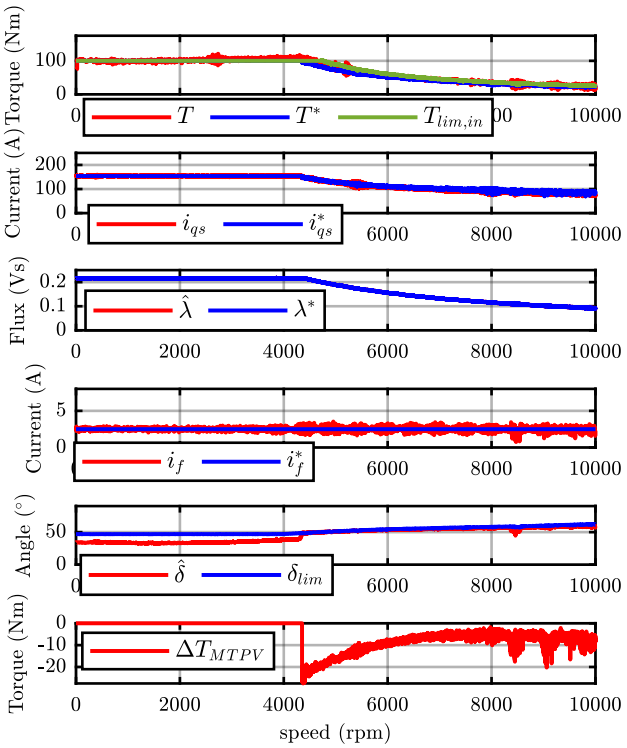


Fig. 24: MTPV limitation: experimental results.

changed from zero up to the maximum speed of 10000 r/min with an imposed acceleration of approximately 230 r/min/s.

The PI regulator implementing the MTPV limitation has been calibrated using the heuristic procedure hereafter reported. The bandwidth frequency of this PI regulator should be ten times lower than the sampling frequency f_s of the digital controller to ensure small-signal stability of torque regulation. Therefore, the gains of the PI regulator implementing the MTPV limitation have been practically tuned as:

$$f_{b,MTPV} \leq \frac{f_s}{10}; \qquad k_{i,MTPV} = k_{p,MTPV} \cdot 2 \cdot \pi \cdot f_{b,MTPV} \tag{22}$$

The bandwidth frequency $f_{b,MTPV}$ and proportional gain $k_{p,MTPV}$ have been calibrated using a trial-and-error procedure, aiming to find an acceptable compromise between stable torque controllability and reduced noise on the torque reference. Moreover, it is suggested a value of $f_{b,MTPV}$ lower than the small-signal bandwidth of the stator control loops.

The results are shown in Fig. 24. It is noted that from a speed around 4500 r/min, the load angle limiter (see Fig. 8) implementing the MTPV limitation reduces the torque reference T^* through the correction ΔT_{MTPV}. This way, the observed load angle $\hat{\delta}$ does not overcome the MTPV limit δ_{lim}, avoiding the instability of the DFVC. In conclusion, this test has demonstrated the torque controller's capability to properly limit the load angle (MTPV), avoiding the EESM's pull-out.

V. Conclusion

The article proposed a high-performance torque controller for traction EESM based on a DFVC approach. The proposed solution linearizes the torque regulation in the entire torque-speed range according to the minimization of the overall copper losses due to stator and rotor windings. Thanks to the proposed DFVC approach, high dynamic of torque regulation is obtained since flux and torque production are fully decoupled, as well as the dynamic of the stator variables from that of the rotor current. Furthermore, avoiding direct control of the stator d-axis current mitigates stator–rotor coupling effects, thereby enhancing torque regulation. Besides, the proposed torque controller can deal with variable limits of stator and rotor currents, allowing the integration of the thermal strategies reported in the literature.

The performance of the proposed torque controller has been validated with a commercial EESM for automotive applications. The obtained experimental results confirmed the feasibility of the proposed torque control solution in fully dealing with the high torque/power regions of the machine while ensuring high dynamic performance, including deep FW operations with MTPV limitation. Furthermore, the results demonstrate that the torque regulation linearity is preserved even under significant reduction of stator and rotor current limits.

Potential improvements to the proposed torque controller include the following.

- Implementing the impact of variable stator and rotor windings temperatures to minimize the overall Joule losses in operative conditions different from the rated ones.
- Integrating thermal strategies reported in the literature in the proposed torque controller to perform an active limitation of stator and rotor windings temperature.

Acknowledgment

The authors would like to acknowledge the financial support from the Power Electronics Innovation Center (PEIC) of Politecnico di Torino (www.peic.polito.it).

References

[1] A. El-Refaie and M. Osama, "High specific power electrical machines: A system perspective," *CES Transactions on Electrical Machines and Systems*, vol. 3, no. 1, pp. 88–93, 2019.

[2] A. Krings and C. Monissen, "Review and trends in electric traction motors for battery electric and hybrid vehicles," in *2020 International Conference on Electrical Machines (ICEM)*, vol. 1, 2020, pp. 1807–1813.

[3] T. Jahns and V. Caliskan, "Uncontrolled generator operation of interior pm synchronous machines following high-speed inverter shutdown," *IEEE Transactions on Industry Applications*, vol. 35, no. 6, pp. 1347–1357, 1999.

[4] C. Rossi, D. Casadei, A. Pilati, and M. Marano, "Wound rotor salient pole synchronous machine drive for electric traction," in *Conference Record of the 2006 IEEE Industry Applications Conference Forty-First IAS Annual Meeting*, vol. 3, 2006, pp. 1235–1241.

[5] F. Graffeo, S. Vaschetto, M. Cossale, M. Kerschbaumer, E. C. Bortoni, and A. Cavagnino, "Cylindrical wound-rotor synchronous machines for traction applications," in *2020 International Conference on Electrical Machines (ICEM)*, vol. 1, 2020, pp. 1736–1742.

[6] F. Graffeo, S. Vaschetto, A. Tenconi, and A. Cavagnino, "No-load characteristic computation for wound field synchronous propulsion motors," in *2023 IEEE International Conference on Electrical Systems for Aircraft, Railway, Ship Propulsion and Road Vehicles and International Transportation Electrification Conference (ESARS-ITEC)*, 2023, pp. 1–6.

Authorized licensed use limited to: Politecnico di Torino. Downloaded on March 19,2026 at 08:41:58 UTC from IEEE Xplore. Restrictions apply.
© 2026 IEEE. All rights reserved, including rights for text and data mining and training of artificial intelligence and similar technologies. Personal use is permitted, but republication/redistribution requires IEEE permission. See https://www.ieee.org/publications/rights/index.html for more information.

This article has been accepted for publication in IEEE Transactions on Industry Applications. This is the author's version which has not been fully edited and content may change prior to final publication. Citation information: DOI 10.1109/TIA.2026.3675223

[7] ——, "Fast sizing procedure for salient-pole wound field synchronous motors for transportation electrification," in *2023 IEEE International Electric Machines and Drives Conference (IEMDC)*, 2023, pp. 1–7.

[8] M. Märgner and W. Hackmann, "Control challenges of an externally excited synchronous machine in an automotive traction drive application," in *2010 Emobility - Electrical Power Train*, 2010, pp. 1–6.

[9] G. Friedrich, "Comparative study of three control strategies for the synchronous salient poles and wound rotor machine in automotive applications with on board energy," in *1994 Fifth International Conference on Power Electronics and Variable-Speed Drives*, 1994, pp. 706–709.

[10] C. D. Nguyen and W. Hofmann, "Self-tuning adaptive copper-losses minimization control of externally excited synchronous motors," in *2014 International Conference on Electrical Machines (ICEM)*, 2014, pp. 897–902.

[11] R. Breda, G. Andrioli, S. Calligaro, and R. Petrella, "Extended mtpa and flux-weakening control with total copper loss minimisation and transient torque compensation for wound-rotor synchronous machines," in *2023 IEEE Energy Conversion Congress and Exposition (ECCE)*, 2023, pp. 4829–4836.

[12] R. Breda, N. Andreon, S. Calligaro, and R. Petrella, "Comprehensive flux-weakening and analytical extended mtpa control featuring transient torque compensation for hybrid excited synchronous machines," in *2024 IEEE Energy Conversion Congress and Exposition (ECCE)*, 2024, pp. 6417–6424.

[13] C. Zaghrini, G. Khoury, M. Fadel, R. Ghosn, and F. Khatounian, "Minimum copper losses per torque optimization on electrically excited synchronous motors for electric vehicles applications," in *2022 IEEE 20th International Power Electronics and Motion Control Conference (PEMC)*, 2022, pp. 661–666.

[14] R. Breda, E. Colavitto, S. Calligaro, R. Petrella, and B. Sarlioglu, "Model predictive control for wound rotor synchronous machines based on closed-form solution and fixed switching frequency," in *2024 IEEE Energy Conversion Congress and Exposition (ECCE)*, 2024, pp. 6349–6356.

[15] D. Casadei, F. Profumo, G. Serra, and A. Tani, "Foc and dtc: two viable schemes for induction motors torque control," *IEEE Transactions on Power Electronics*, vol. 17, no. 5, pp. 779–787, 2002.

[16] L. Geier, S. Goehner, J. Stoss, A. Liske, and M. Hiller, "A novel highly dynamic torque control scheme for electrically excited synchronous machines," in *2024 IEEE 9th Southern Power Electronics Conference (SPEC)*, 2024, pp. 1–7.

[17] A. K. Jain and V. T. Ranganathan, "Modeling and field oriented control of salient pole wound field synchronous machine in stator flux coordinates," *IEEE Transactions on Industrial Electronics*, vol. 58, no. 3, pp. 960–970, 2011.

[18] Y. Nie, I. P. Brown, and D. C. Ludois, "Deadbeat-direct torque and flux control for wound field synchronous machines," *IEEE Transactions on Industrial Electronics*, vol. 65, no. 3, pp. 2069–2079, 2018.

[19] Y. Nie, D. C. Ludois, and I. P. Brown, "Deadbeat-direct torque and flux control of wound field synchronous machine at low sampling to fundamental frequency ratios," *IEEE Transactions on Industry Applications*, vol. 55, no. 4, pp. 3813–3822, 2019.

[20] Y. Kim and K. Nam, "Copper-loss-minimizing field current control scheme for wound synchronous machines," *IEEE Transactions on Power Electronics*, vol. 32, no. 2, pp. 1335–1345, 2017.

[21] M.-R. Park, D.-M. Kim, Y.-H. Jung, M.-S. Lim, and J.-P. Hong, "Modeling, design and control of wound-field synchronous motor for high energy efficiency of electric vehicle," in *2019 IEEE Energy Conversion Congress and Exposition (ECCE)*, 2019, pp. 3960–3967.

[22] S. Müller and N. Parspour, "Applying a measurement-based iron loss model to an efficiency optimized torque control of an electrically excited synchronous machine," in *2020 International Conference on Electrical Machines (ICEM)*, vol. 1, 2020, pp. 779–785.

[23] E. Gundabattini, A. Mystkowski, A. Idzkowski, R. S. R., and D. G. Solomon, "Thermal mapping of a high-speed electric motor used for traction applications and analysis of various cooling methods—a review," *Energies*, vol. 14, no. 5, 2021. [Online]. Available: https://www.mdpi.com/1996-1073/14/5/1472

[24] P. Roy, M. Towhidi, F. Ahmed, A. J. Bourgault, S. Mukandan, A. Balamurali, and N. C. Kar, "A comprehensive review of thermal design and analysis of traction motors," in *2019 IEEE 28th International Symposium on Industrial Electronics (ISIE)*, 2019, pp. 203–208.

[25] S. Nategh, A. Boglietti, D. Barber, Y. Liu, and R. Brammer, "Thermal and manufacturing aspects of traction motors potting: A deep experimental evaluation," *IEEE Transactions on Energy Conversion*, vol. 35, no. 2, pp. 1026–1035, 2020.

[26] D. T. Machacek, K. Barhoumi, J. M. Ritzmann, T. Huber, and C. H. Onder, "Multi-level model predictive control for the energy management of hybrid electric vehicles including thermal derating," *IEEE Transactions on Vehicular Technology*, vol. 71, no. 10, pp. 10 400–10 414, 2022.

[27] J. Lemmens, P. Vanassche, and J. Driesen, "Optimal control of traction motor drives under electrothermal constraints," *IEEE Journal of Emerging and Selected Topics in Power Electronics*, vol. 2, no. 2, pp. 249–263, 2014.

[28] A. Ranjan, D. V. Bhaskar, P. Kumar, and U. R. Muduli, "Comprehensive analysis of thermal effects on pmsm drive control in small commercial vehicles," in *2024 IEEE International Conference on Power Electronics, Drives and Energy Systems (PEDES)*, 2024, pp. 1–6.

[29] J. Lemmens, J. Driesen, and P. Vanassche, "Thermal management in traction applications as a constraint optimal control problem," in *2012 IEEE Vehicle Power and Propulsion Conference*, 2012, pp. 36–41.

[30] G. Pellegrino, R. Bojoi, and P. Guglielmi, "Unified direct-flux vector control for ac motor drives," *IEEE Transactions on Industry Applications*, vol. 47, no. 5, pp. 2093–2102, 2011.

[31] S. Rubino, R. Bojoi, E. Armando, and A. Tenconi, "Deadbeat direct flux vector control of surface permanent magnet motor drives," *IEEE Transactions on Industry Applications*, vol. 56, no. 3, pp. 2685–2699, 2020.

[32] H. A. A. Awan, M. Hinkkanen, R. Bojoi, and G. Pellegrino, "Stator-flux-oriented control of synchronous motors: A systematic design procedure," *IEEE Transactions on Industry Applications*, vol. 55, no. 5, pp. 4811–4820, 2019.

[33] A. Ionta, S. Rubino, F. Mandrile, F. Graffeo, R. Bojoi, and E. Armando, "Direct flux vector control of electrically excited synchronous machines for electrical vehicles," in *2024 IEEE Energy Conversion Congress and Exposition (ECCE)*, 2024, pp. 6431–6438.

[34] J. K. Nøland, S. Nuzzo, A. Tessarolo, and E. F. Alves, "Excitation system technologies for wound-field synchronous machines: Survey of solutions and evolving trends," *IEEE Access*, vol. 7, pp. 109 699–109 718, 2019.

[35] F. Stella, S. Rubino, E. Vico, R. Bojoi, and E. Armando, "Excitation sic converter for electrically excited traction synchronous motor using rotary transformer and field rotor current estimator," in *2024 IEEE Energy Conversion Congress and Exposition (ECCE)*, 2024, pp. 2000–2006.

[36] S. Rubino, L. Tolosano, F. Mandrile, E. Armando, and R. Bojoi, "Flux polar control (fpc): A unified torque controller for ac motor drives," *IEEE Transactions on Industry Applications*, vol. 59, no. 4, pp. 4140–4163, 2023.

[37] B. Stumberger, G. Stumberger, D. Dolinar, A. Hamler, and M. Trlep, "Evaluation of saturation and cross-magnetization effects in interior permanent-magnet synchronous motor," *IEEE Transactions on Industry Applications*, vol. 39, no. 5, pp. 1264–1271, 2003.

[38] A. Hava, R. Kerkman, and T. Lipo, "Simple analytical and graphical methods for carrier-based pwm-vsi drives," *IEEE Transactions on Power Electronics*, vol. 14, no. 1, pp. 49–61, 1999.

[39] A. Vagati, M. Pastorelli, G. Franceschini, and V. Drogoreanu, "Flux-observer-based high-performance control of synchronous reluctance motors by including cross saturation," *IEEE Transactions on Industry Applications*, vol. 35, no. 3, pp. 597–605, 1999.

[40] G. Pellegrino, R. I. Bojoi, P. Guglielmi, and F. Cupertino, "Accurate inverter error compensation and related self-commissioning scheme in sensorless induction motor drives," *IEEE Transactions on Industry Applications*, vol. 46, no. 5, pp. 1970–1978, 2010.

[41] I. Bojoi, E. Armando, G. Pellegrino, and S. Rosu, "Self-commissioning of inverter nonlinear effects in ac drives," in *2012 IEEE International Energy Conference and Exhibition (ENERGYCON)*, 2012, pp. 213–218.

[42] S.-Y. Kim, C. Choi, K. Lee, and W. Lee, "An improved rotor position estimation with vector-tracking observer in pmsm drives with low-resolution hall-effect sensors," *IEEE Transactions on Industrial Electronics*, vol. 58, no. 9, pp. 4078–4086, 2011.

[43] E. Armando, R. Bojoi, P. Guglielmi, G. Pellegrino, and M. Pastorelli, "Experimental identification of the magnetic model of synchronous machines," *IEEE Transactions on Industry Applications*, vol. 49, no. 5, pp. 2116–2125, 2013.

[44] S. Goehner, J. Stoss, M. Brodatzki, B. Bachowsky, A. Liske, J. Kolb, and M. Hiller, "Combining locked rotor and steady state tests for eesm flux linkage identification," in *2024 IEEE 9th Southern Power Electronics Conference (SPEC)*, 2024, pp. 1–6.

[45] F. Graffeo, S. Rubino, M. J. Molina, S. Vaschetto, and A. Tenconi, "Efficiency mapping of electrically excited synchronous motors with different control strategies," in *2025 IEEE Workshop on Electrical Machines Design, Control and Diagnosis (WEMDCD)*, 2025, pp. 1–6.

Authorized licensed use limited to: Politecnico di Torino. Downloaded on March 19,2026 at 08:41:58 UTC from IEEE Xplore. Restrictions apply.
© 2026 IEEE. All rights reserved, including rights for text and data mining and training of artificial intelligence and similar technologies. Personal use is permitted, but republication/redistribution requires IEEE permission. See https://www.ieee.org/publications/rights/index.html for more information.

This article has been accepted for publication in IEEE Transactions on Industry Applications. This is the author's version which has not been fully edited and content may change prior to final publication. Citation information: DOI 10.1109/TIA.2026.3675223



Alessandro Ionta (Student Member, IEEE) was born in Rome, Italy, in 1999. He received the bachelor degree in electrical engineering and the master degree in mechatronic engineering, in 2020 and 2022, respectively, from the Politecnico di Torino, Torino, Italy, where he is currently working toward the Ph.D degree with Dipartimento Energia "G. Ferraris". His Ph.D topic relates on advanced control and modeling of electrical motors for traction applications, with a particular focus on electrically excited synchronous motors.



Sandro Rubino (Senior Member, IEEE) received the M.Sc. and PhD degrees in electrical engineering from Politecnico di Torino, Torino, Italy, in 2014 and 2019, respectively. He is currently an Associate Professor at the Energy Department "G. Ferraris" of Politecnico di Torino. His research activities include modelling and controlling multiphase electrical machines and high-performance motor drives. Prof. Sandro Rubino currently serves as the Secretary of the Industrial Drive Committee (IDC) of the IEEE Industry Applications Society (IAS). Also, he is an Associate Editor of IEEE Transactions on Industry Applications and IEEE Journal of Emerging and Selected Topics in Power Electronics. Prof. Sandro Rubino received four paper awards from IAS-IDC and two PhD thesis awards for the design and validation of advanced torque controllers for traction and propulsion motors. He is involved in many research projects with industry aimed at technology transfer from academia.



Federica Graffeo (S'20–M'24) received the B.Sc. degree in energy engineering from the Università degli Studi di Palermo, Palermo, Italy, in 2017, and the M.Sc. and Ph.D. degrees in electrical engineering from the Politecnico di Torino, Turin, Italy, in 2020, and 2023, respectively. She is currently an Assistant Professor with the Dipartimento Energia "G. Ferraris," Politecnico di Torino. Her research interests include electromagnetic and thermal design of synchronous electrical machines for transportation applications, with a particular focus on wound field synchronous motors. Dr. Graffeo serves as a reviewer for some IEEE TRANSACTIONS and international conferences.



Fabio Mandrile (Member, IEEE) received the M.Sc. and Ph.D. degrees in electrical engineering from Politecnico di Torino, Torino, Italy, in 2017 and 2021, respectively. His main research interests include virtual synchronous generators, power electronics for grid connected applications, the experimental characterization of converters, and motor drives.



Radu Bojoi (Fellow, IEEE) received the M.Sc.in electrical engineering from the Technical University of Iasi, Iasi, Romania,in 1993, and the Ph.D. degree in electrical engineering from the Politecnico di Torino, Torino, Italy, in 2002. He is currently a Full Professor of Power Electronics and Electrical Drives with the Energy Department "G. Ferraris" and Chairman of the Power Electronics Innovation Center, Politecnico di Torino. Dr. Bojoi is the recipient of ten IEEE paper awards, being co-author of more than 200 papers covering electrical drives and power electronics for industrial applications, transportation electrification, power quality, and home appliances. Prof. Bojoi is involved in many research projects with industry aiming at obtaining new products involving emerging technologies.



Eric Giacomo Armando (Senior Member, IEEE) received the M.Sc. and Ph.D. degrees in electrical engineering from Politecnico di Torino, Turin, Italy, in 2002 and 2008, respectively. He is currently a Full Professor of power converters, electrical machines, and drives with Politecnico di Torino . He is the co-author of numerous Journal Papers and three Patents. His research interests include power electronics and high performance AC motor drives. He was the recipient of three awards for innovation, one paper award from the Power Electronics Technical Committee of the IEEE Industrial Electronics Society, and one paper award from the Industrial Drives Committee of the IEEE Industry Applications Society.

Authorized licensed use limited to: Politecnico di Torino. Downloaded on March 19,2026 at 08:41:58 UTC from IEEE Xplore. Restrictions apply.
© 2026 IEEE. All rights reserved, including rights for text and data mining and training of artificial intelligence and similar technologies. Personal use is permitted, but republication/redistribution requires IEEE permission. See https://www.ieee.org/publications/rights/index.html for more information.